Predicting the disruption by UO_2^{2+} of a protein-ligand interaction

Olivier Pible,* Claude Vidaud, Sophie Plantevin, Jean-Luc Pellequer, and Eric Quéméneur

CEA, DSV, IBEB, SBTN, Bagnols-sur-Cèze, F-30207, France

Received 26 May 2010; Revised 30 August 2010; Accepted 4 September 2010
DOI: 10.1002/pro.501
Published online 14 September 2010 proteinscience.org

Abstract: The uranyl cation (UO_2^{2+}) can be suspected to interfere with the binding of essential metal cations to proteins, underlying some mechanisms of toxicity. A dedicated computational screen was used to identify UO_2^{2+} binding sites within a set of nonredundant protein structures. The list of potential targets was compared to data from a small molecules interaction database to pinpoint specific examples where UO_2^{2+} should be able to bind in the vicinity of an essential cation, and would be likely to affect the function of the corresponding protein. The C-reactive protein appeared as an interesting hit since its structure involves critical calcium ions in the binding of phosphorylcholine. Biochemical experiments confirmed the predicted binding site for UO_2^{2+} and it was demonstrated by surface plasmon resonance assays that UO_2^{2+} binding to CRP prevents the calcium-mediated binding of phosphorylcholine. Strikingly, the apparent affinity of UO_2^{2+} for native CRP was almost 100-fold higher than that of Ca^{2+}. This result exemplifies in the case of CRP the capability of our computational tool to predict effective binding sites for UO_2^{2+} in proteins and is a first evidence of calcium substitution by the uranyl cation in a native protein.

Keywords: uranium; uranyl ion; computational screening; molecular docking; modeling; C-reactive protein; surface plasmon resonance

Introduction

Metal cations are involved in many biochemical processes, and are common when focusing on proteins. Divalent cations in particular are found in many mechanisms, playing either structural or catalytic roles, or acting as mediators in protein-ligand complexes.[1–4]

However, some naturally abundant cations such as the uranyl ion (UO_2^{2+}) have never been reported as integral parts in any biochemical system. Considering the large industrial use of uranium, UO_2^{2+} has been the subject of many toxicological studies that revealed its ability to interact with a large variety of biochemical targets. Recent investigations included analysis of specific metal carriers,[5–8] of human serum proteins,[9,10] and both proteomic and transcriptomic studies to identify proteins related to cellular impacts.[11,12]

UO_2^{2+} is reported to deposit into bone with a metabolism similar to that of calcium,[13] making ionic substitution a plausible hypothesis for some biochemical features of uranium. Le Clainche and Vita[14] used the calcium binding Site I of the protein calmodulin as a template to design a peptide binding the uranyl cation. However, the direct competition of the uranyl cation at a calcium binding site of a native protein has to our knowledge not yet been reported. To probe this hypothesis, a computational tool was mandatory. Methods have been developed to detect calcium or zinc binding sites in proteins.[15–18] For the uranyl ion, we used in this study the only UO_2^{2+}-docking tool available, which we described previously.[19]

Abbreviations: BSA-PC, phosphorylcholine hapten conjugated to bovin serum albumin; CRP, C-reactive protein; pCRP, pentameric CRP; mCRP, monomeric CRP; IUM, uranyl ion PDB identifier; PC, phosphorylcholine (or phosphocholine); PDB, Protein Data Bank; SMID, Small Molecule Interaction Database; SPR, Surface Plasmon Resonance.

Additional supporting information may be found in the online version of this article.

**Correspondence to:* Olivier Pible, CEA Life Sciences Division, iBEB/SBTN, BP17171, F-30207 Bagnols sur Cèze, France. E-mail: olivier.pible@cea.fr

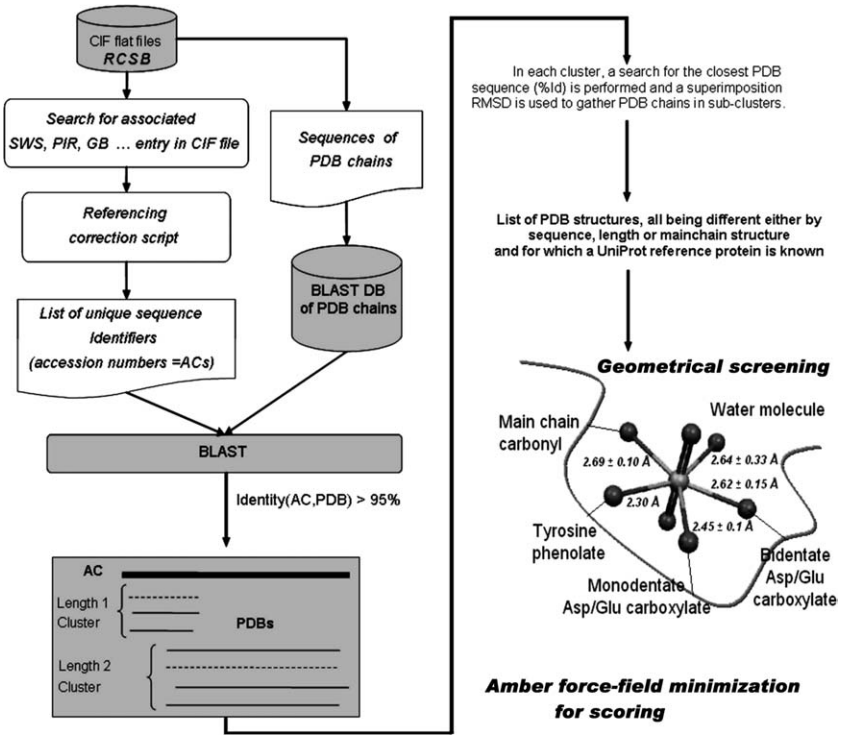

Figure 1. Selection of PDB subset, clustering, and docking. Selection of the least mutated PDB protein chains matching each portion of wild type protein sequences, after discarding chains of near identical structure. 12837 PDB unique IDs were selected as the database subset. A two-stage screening method identified and scored UO_2^{2+} chelation sites in these structures.

Our computational method relies on rigid mainchain and full sidechain flexibility to predict UO_2^{2+} interaction sites in protein of known 3D-structures. While a few metalloproteins bind metal ions with large conformational changes, most metalloproteins impose constrained metal site geometries, with marginal fluctuation of their overall structure between metal-free and metal-bound states.[20,21] In such cases, protein ligands are often observed to interact in a metal-dependent mode, that is, with direct coordination with the metal ions. Metal substitution is then expected to change protein-ligand binding properties.

Our screening methodology was applied to a subset of the Protein Data Bank (PDB).[22] Results were then compared to data from the Small Molecule Interaction Database (SMID),[23] to pinpoint specific calcium dependant interactions between proteins and small molecules likely to be inhibited by UO_2^{2+}substitution. The C-reactive protein (CRP), a predicted template, was experimentally characterized to demonstrate this novel mode of action.

Results

Screening of PDB for UO_2^{2+} sites near protein ligands and metal cations

Sequences from protein sequence databases, such as UniProtKB/Swiss-Prot,[24] and from the PDB usually differ.[25,26] Missing signal peptides, missing domains or unresolved exposed loops, and redundancies due to site mutations are common discrepancies.

A simple selection scheme was used to select structures representative of native proteins and to reduce the computer screening time as detailed in Figure 1. This led to the selection of 12837 PDB unique IDs as the database subset. PDB entries corresponding to the same protein were kept in the subset despite nearly identical chain sequences and length, as long as existing or missing ligands caused slight structural variations. In such cases, the Cα root mean square deviations (RMSD) threshold used was 0.5814, corresponding to 80% similarity according to Lesk and Chothia.[27]

Our search algorithm[19] was then applied to each of those structures, resulting in a set of possible chelation sites with corresponding scores based on energy minimization using the Amber force-field. The score distribution of the raw screening results is displayed in Figure 2. The calculated score [Eq. (1)] took into account both the deformation energy of the protein (E_{def}, difference of internal energy between the complexed and uncomplexed forms), the protein-UO_2^{2+} interaction energy ($E_{\mathrm{P\text{-}IUM}}$, where IUM is the PDB identifier for UO_2^{2+}) plus nonbonded terms related to water-protein and water-uranium interactions (E_{PUW}).

$$\mathrm{Score} = \mathrm{E_{def}} + \mathrm{E_{P-IUM}} + \mathrm{E_{PUW}} \qquad (1)$$

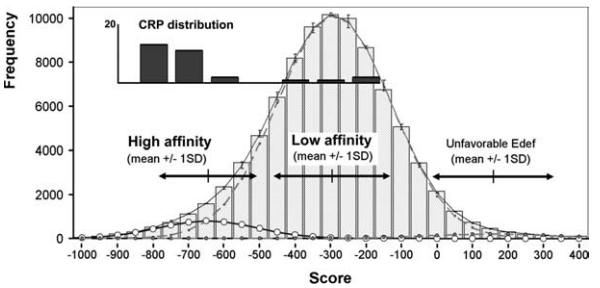

Figure 2. Distribution of screening raw scores, fit with the sum of three Gaussian functions (thin black line). Black arrows indicate the mean of each fit and one standard deviation around the mean. The first fit from the left (bold black line, round black mark) is attributed to a population with high affinity for UO_2^{2+} (mean = −647, SD = 137); the center fit (dashed grey line) is attributed to a low affinity population (mean = −291, SD = 160); and the last fit on the right (dashed grey line, round grey mark) is attributed to a population with unfavorable deformation energy for binding such a ligand (mean = 160, SD = 179).

This score is the sum of enthalpic energy terms, expressed in kcal/mol. Being similar to an energy function, the lower the value, the higher the propensity for interaction between the protein and the uranyl ion at each particular site. The best fit for the score distribution was obtained with a mixture of 3 Gaussian curves (Fig. 2).

Selection of an experimental target

12% of the proteins sites detected in our scheme were already populated with divalent cations: Ca^{2+} (8.1%), Mg^{2+} (1.6%), Mn^{2+} (1.0%), Zn^{2+} (0.4%), Co^{2+} (0.2%), and so forth. Proteins interacting with small molecules in a metal-dependent mode were also numerous. Table I reports such target proteins with high potential for UO_2^{2+}binding, that is, with a SMID ligand detected at less than 3 Å from the position of the uranyl cation.

Four proteins attracted our attention since they all display a putative UO_2^{2+}binding site in the binding pocket for both an organic and a metallic ligand: CRP, fucose binding lectin II, DHBP synthase, and MBP-C. They represented testable models for our initial hypothesis that the uranyl ion might be a potent interferent of the formation of physiological complex.

Based on its score and availability, this study will focus on CRP. It forms a ring-shaped structure homopentamer (pCRP, 115kDa), which can interact with various types of molecules. One side of the ring can interact with polycationic compounds, carbohydrates (D-galactose related structures), or with phosphorylcholine (PC) in a calcium dependent manner. Attachment to the surface of pathogens, or binding to lyso-phosphatidylcholine of apoptotic/necrotic cells results in the activation of the classical complement cascade, through C1q binding on the other side of the molecule.[28–30]

The analysis of several structures revealed that the binding of Ca^{2+} and PC to pCRP involves only minor and local conformational rearrangements. The Cα RMSD between calcium-free (PDB 1LJ7[31]) versus calcium-bound (1GNH[32]) structures, and of calcium-free versus Ca^{2+}/PC-bound (1B09[33]) structures were measured at 0.33 and 0.44 Å, respectively, using 199 amino acid residues from monomer A. This was also true at the level of the quaternary structures, with Cα RSMD of 0.87 and 0.81 Å, respectively, over the 998 amino acid residues of the five monomers.

On the other hand, monomerization of pCRP to mCRP is associated with significant conformational changes.[34] mCRP does not spontaneously bind PC,[34–36] and was thus used as a control for nonspecific binding experiments in some of our following experiments.

Reported inhibitors of CRP–PC interaction are phosphorylcholine derivatives, including phosphate containing molecules and detergents [37,38]. Mg^{2+} was also documented as a marginal CRP ligand.[35,39,40]

Our results suggest that UO_2^{2+} is a potent ligand. Its mean score of −783 for all the selected sites corresponds to 85% probability of belonging to the "High affinity" population according to Bayes' inversion rule (see Fig. 2, distribution of scores). All predicted sites were located in the calcium-binding area of one of the chains, in a geometry which prevents phosphorylcholine from sterically coexisting with the uranyl ion.

The binding of UO_2^{2+} to CRP was demonstrated by dialysis at equilibrium in the absence of Ca^{2+}. A UO_2^{2+}-loaded protein solution was extensively dialyzed for 5 h. The UO_2^{2+} content was then quantified by inductively coupled plasma mass spectrometry (ICP-MS) in two experiments. A ratio of 0.9 ± 0.07 (at 3 SD) equivalents of UO_2^{2+} per protein subunit was measured (see Supporting Information Table SI).

Supporting information Table SII lists all binding sites detected on the three PDB entries associated with CRP (Swiss-Prot AC P02741). CRP calcium binding sites display incomplete coordination spheres, as visible in PDB entry 1GNH where only calcium atoms and no PC are present in the crystal. Half of the first coordination shells of Ca^{2+} are populated with protein atoms, with labile water or solvent molecules not clearly visible at 3 Å resolution. These solvent-exposed half spheres of coordination are important for PC binding.

Pronase assay: UO_2^{2+} protects CRP better than Ca^{2+}

Sidechains involved in calcium binding are predicted to be also involved in UO_2^{2+} binding. Kinoshita *et al.* reported how Ca^{2+} binding protects the loop

Table I. *Subset List of Target Proteins*

Swiss-Prot accession number	Protein name	Sequence length	Pfam families	Total #PDBs	Post clustering #PDBs	PDB files with at least one accepted score[a]	SMID molecules close to uranyl hit locations	Mean of gaussian fit of scores	SD of gaussian fit of scores	Percentage of hits with score higher than mean 1SD
P09803	Epithelial cadherin	884	Cadherin_pro; Cadherin; Cadherin_C	**7**	**6**	**1Q1P**; **1FF5**; **1EDH**	Ca	−841	41	8%
P0A6A8	Acyl carrier protein	78	PP-binding	**7**	**3**	1L0H; **1L0I**	Zn	−828	63	21%
P42566	Epidermal growth factor receptor substrate 15	896	efhand	**4**	**4**	**1F8H**;1EH2;1FF1; 1C07	Ca	−821	56	30%
P0A5N0	Aminoglycoside 2′-N-acetyltransferase	181	Acetyltransf_1	**4**	**2**	**1M4I**; 1M44	Kanamycin	−780	60	8%
P02619	Parvalbumin beta	107	efhand	**6**	**5**	**3PAL;** 1PVB; 4PAL; 1PAL; 2PVB	Ca	−761	88	8%
P02741	C-reactive protein	224	Pentraxin	**3**	**3**	**1GNH;** 1LJ7; **1B09**	Ca; PC	−755	60	20%
P37819	Proclavaminate amidinohydrolase	313	Arginase	2	2	**1GQ6; 1GQ7**	Mn	−749	89	29%
P09860	Troponin C, slow skeletal and cardiac muscles	161	efhand	**8**	**6**	**2CTN; 1DTL; 1FI5; 1AJ4; 3CTN;** 1LA0	Ca	−728	98	9%
P00582	DNA polymerase I	928	5_3_exonuc_N; 3_5_exonuc; DNA_pol_A	14	4	1KFD; **2KFZ**	Zn	−700	49	17%
Q9HYN5	Fucose-binding lectin PA-IIL	115	PA-IIL (lectinII)	**12**	**2**	1OUS; **1OXC**	Ca; FUC	−673	59	10%
P20942	Phosducin	246	Phosducin	**3**	**3**	**2TRC; 1B9X**	Gd	−669	37	0%
Q60364	3,4-dihydroxy-2-butanone 4-phosphate synthase	227	DHBP_synthase	**3**	**2**	**1PVW; 1PVY**	Zn; Ca; Pi; R5P	−666	38	0%
Q64537	Calpain small subunit 1	270	efhand	**5**	**4**	1AJ5; **1DVI;** 1NP8	Ca	−659	51	23%
P08661	Mannose-binding protein C	244	Collagen; Lectin_C	**13**	**4**	**1KZA; 1RDO; 1RDL;** 1BV4	Ca; man	−651	41	26%

[a] PDB entries in bold were found with hetero atoms (excluding water) less than 3 Å away from uranyl hit locations.

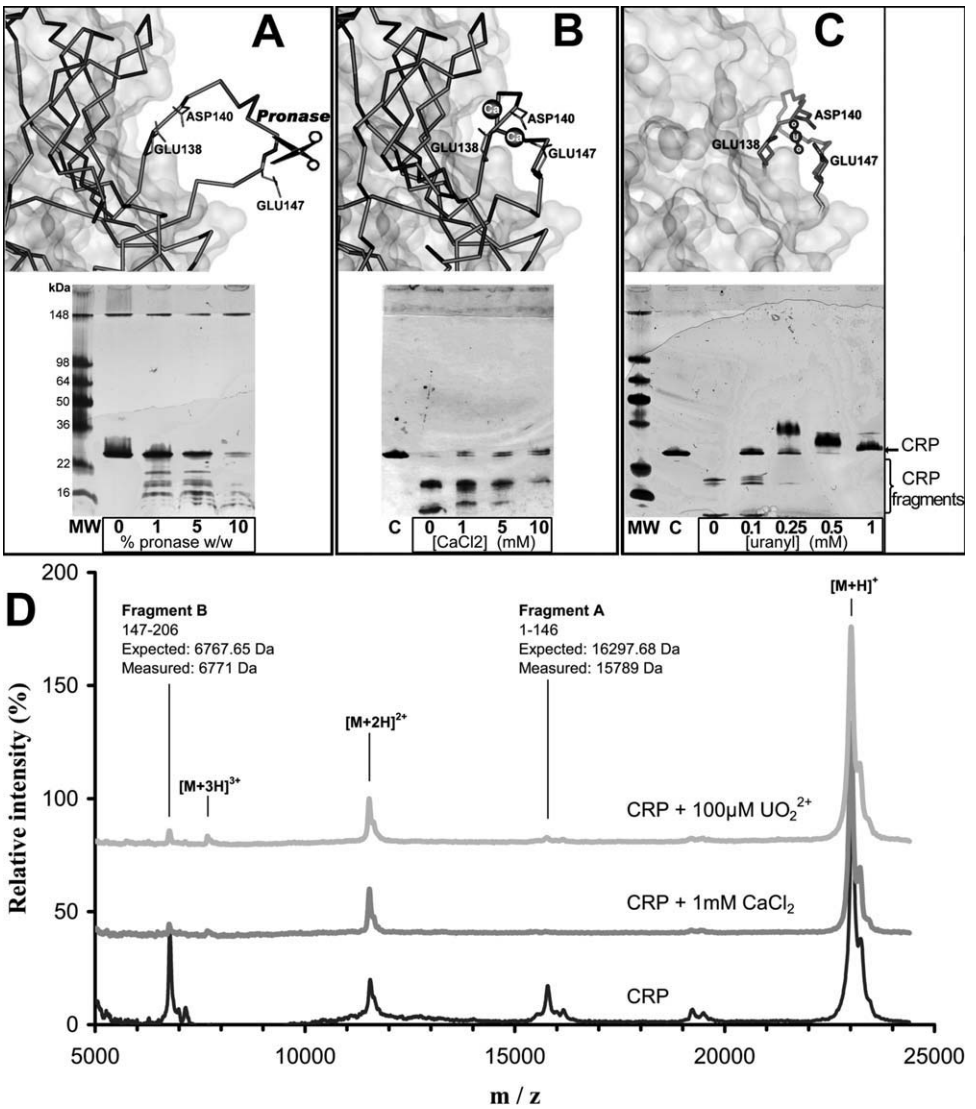

Figure 3. Conformational sensitivity of CRP to digestion with pronase. **A**: Top: without bound calcium atoms, the $CRP_{138–148}$ loop is largely exposed to solvent (IGNH chain D). Bottom: electrophoresis gel of CRP (200 μg/mL) digestion at a fixed $CaCl_2$ concentration (1 mM) and an increasing concentration of pronase, which promotes CRP (23 kDa) digestion. **B**: Top: in the presence of two bound calcium atoms, the $CRP_{138–148}$ loop is less exposed to the solvent (1GNH chain C). Bottom: electrophoresis gel of CRP (200 μg/mL) digestion at a fixed concentration of pronase (5%W/W) and an increasing concentration of $CaCl_2$. Calcium precludes CRP digestion by pronase [41]. **C**: Top: predicted binding site geometry of chelated UO_2^{2+} geometry on CRP chain C (IGNH). The side chains responsible for calcium chelation in CRP are also involved in UO_2^{2+} binding. Bottom: protection against pronase digestion of CRP (200 μg/mL) with increasing concentrations of the uranyl ion. Electrophoresis results represent at least two independent silver staining experiments. **D**: MALDI-TOF mass spectra of CRP. CRP was incubated without metal (black), with 1 mM $CaCl_2$ (dark grey) and 100 μM UO_2^{2+} (light grey) prior to pronase digestion. Relative intensity was set at 100% for the $[M+H]^+$ peak. $[M+H]^+$, $[M+2H]^{2+}$, and $[M+3H]^{3+}$ are assigned to mono, doubly, and triply charged intact CRP peaks, fragments A and B are pronase digestion products. Calcium and UO_2^{2+} spectra show very similar peak distribution, with near disappearance of digestion products in agreement with electrophoresis results, implying that the conformation of the metal-bound CRP loop is similar for both metals.

involving residues 141 to 148 against proteolytic cleavage by pronase (cleavage at Glu147).[41] UO_2^{2+} capability of preventing digestion was thus tested.

The protease concentration was adjusted by monitoring CRP digestion at various pronase/CRP ratios (1, 5 and 10% w/w), in the presence of 1 mM Ca^{2+} [Fig. 3(A)]. A 5% ratio was selected for subsequent experiments, as a trade-off between intact protein at 23 kDa, and the 16 kDa and 6.5 kDa fragments. In accordance with Kinoshita *et al.*,[41] there was a clear decrease in proteolysis susceptibility when calcium concentrations increased [Fig. 3(B)].

Pronase was neither inactivated by calcium nor by UO_2^{2+}, as verified using human albumin as a control under various concentrations of $CaCl_2$ (1 to 5 mM) and UO_2^{2+} (0.1 to 1 mM). Nonspecific

electrostatic interactions in electrophoresis experiments were also tested using Mg^{2+}. CRP was not protected from proteolysis at Mg^{2+} concentration up to 10 mM (data not shown).

Figure 3(C) showed that UO_2^{2+} protects CRP against pronase more efficiently than Ca^{2+}, since digestion profiles appeared similar at 1 mM Ca^{2+} and 0.1 mM UO_2^{2+}. The masses of fragments obtained in MALDI-TOF-MS experiments confirmed the expected cleavage site in the calcium binding loop.[41] Spectra obtained were similar whenever Ca^{2+} or UO_2^{2+} was used [Fig. 3(D)], indirectly confirming identical binding sites for both cations.

Interaction of Ca and PC with CRP

Surface plasmon resonance (SPR) was used to study the binding of PC to CRP. The setup involved immobilized PC, under the form of a PC-BSA conjugate covalently linked to the sensor chip, and circulating pCRP, and the reciprocal setting. Under both conditions the absence of Ca^{2+} gave no measurable signal, while increasing its concentration proportionally enhanced the signal to reach a plateau at 2 mM $CaCl_2$, as previously reported.[39] Observed signals were consistent with a maximal binding of one PC-BSA molecule per CRP pentamer. The absence of calcium in the dissociation buffer caused the immediate release of bound molecules.

Binding levels were on average and consistently seven times lower at 50 μM $CaCl_2$ compared to those measured in the presence of 2 mM $CaCl_2$ (data not shown). Because both calcium cations are needed for PC binding, a rough estimate of K_D (Ca-CRP) can be drawn from this ratio, supposing equal affinity[41] and independency of calcium binding to both sites. A 1/7 ratio for PC binding implies that individual calcium site occupancy is $(1/7)^{0.5}$, relating to the Y/Rmax value in the first term of Eq. (2) depicting the law of mass action. At X = 50 μM $CaCl_2$, we deduced a K_D value of 82 μM. This agrees with reported K_D, in the range of 50–78.1 μM.[39,41,42]

We also estimated the binding affinity of PC to CRP. The published K_D values are from 5 to 18 μM for human CRP.[39,40,43,44] We consistently obtained K_D values between 0.4 and 1 μM for CRP interaction with PC-BSA in the presence of 50 μM Ca^{2+}, whatever the settings and the sensor chips. Since the functionalization ratio is 10 PC molecules per BSA protein, avidity for the five binding sites of pCRP could account for the 10-fold difference with the reported affinity for free PC/CRP. Binding saturation was reached when CRP concentration was raised to 10 μM (Supporting Information Fig. S1).

Inhibition experiments: UO_2^{2+} as a potent inhibitor

As expected, EDTA displayed a marked inhibition of PC binding. Free PC was also found to inhibit CRP binding to immobilized PC-BSA, with an IC50 below 0.1 μM at 50 μM Ca^{2+} (data not shown). $MgCl_2$ was also assayed at concentrations up to 1 mM (as a reminder, body concentration is ~ 0.5 mM[45]). Neither inhibition nor enhancement of CRP-PC interaction was observed despite a molar excess of 20 over Ca^{2+}. This result suggested that Mg^{2+} cannot replace Ca^{2+} cations in the CRP calcium binding sites. The previously reported magnesium binding to CRP[35,40] is thus assumed to occur either in the calcium site with a K_D value in the millimolar range at best, or in different binding sites.

UO_2^{2+} was tested in SPR experiments as an inhibitor of circulating PC-BSA binding on a CRP surface [Fig. 4(A)], along with the reversed experiment, in the presence of 50 μM $CaCl_2$ in the buffer. This calcium concentration was considered as a good trade-off between sufficient binding signal and UO_2^{2+} concentrations preserving solubility. In both cases, a strong inhibition was observed, with a half-inhibitory concentration (IC_{50}) of 0.16 μM UO_2^{2+} in the first setup, and 10 μM in the later setup.

The estimation of the refractive index increment (RII) for UO_2^{2+} diacetate diluted in water using SPR was 0.12 cm^3/g instead of 0.18 cm^3/g for proteins, accounting for a possible one third error in stoichiometry estimations (data not shown). The corrected formula used for the prediction of R_{max} for UO_2^{2+} was: $(RUpred)_{max} = RU_M \times (MW_L/MW_M) \times (RII_L/RII_M)$.[46]

Two Ca^{2+} atoms are needed for the binding of PC to a CRP protomer. Figure 4(D,E) show side-by-side the crystal structure of protomer C containing two calcium atoms and a molecule of PC, and the predicted location of the uranyl cation, presumably replacing the calcium atoms. One of the apical oxygen atoms is pointing in the direction normally occupied by the phosphorus atom of PC.

Specificity of the inhibition

Because of the above mentioned differences in IC_{50}, the possibility that binding inhibition could result from either the association of UO_2^{2+} with the phosphate group of PC, or the monomerization of pCRP, was a concern. To rule them out, we used a setup where immobilized pCRP was subjected to various concentrations of UO_2^{2+} (capture step), followed by a dissociation step with running buffer. PC-BSA was then injected, either at the same uranyl ion concentration (Supporting Information Fig. S2) or with no UO_2^{2+} [Fig. 4(B,C)]. Regular association–dissociation stages were recorded. The corresponding binding capacity $(RUpred)_{max}$ was 6.5 RU of UO_2^{2+} for a 1:1 CRP subunit/UO_2^{2+} stoichiometry after RII correction. The observed binding level for UO_2^{2+} on pCRP was in the range 2.5–5 RU, that is, 40 to 80% of available calcium sites. PC-BSA maximal binding

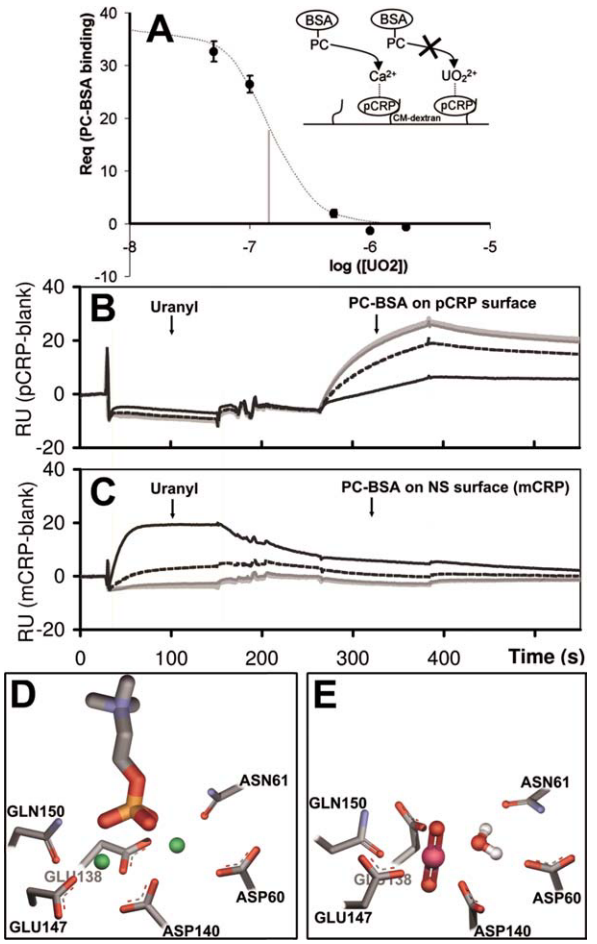

Figure 4. SPR binding inhibition assays. (A) Schematic and SPR data plot of UO_2^{2+} inhibition (IC_{50} = 0.16 μM) of PC-BSA ([PC-BSA] =100nM) binding to CRP (838 immobilized RU). **B**,**C**: SPR sensorgrams showing the effect of a UO_2^{2+} preinjection on the capacity to bind PC-BSA for pCRP (B) and mCRP (C). An increasing concentration of captured UO_2^{2+} (light grey: 0 μM; dark grey: 0.1 μM; dashed black: 0.5 μM; black: 2 μM) only added at a capture stage results in the clear inhibition of PC-BSA (100 nM) binding on native CRP (838RU of immobilized pCRP). mCRP used for nonspecific monitoring shows no UO_2^{2+} dependant signal modulation. In supporting information Figure S2, UO_2^{2+} is also added with PC-BSA, resulting in complete inhibition of PC-BSA binding. **(D)** CRP calcium binding site from PDB structure 1B09 chain C (sticks) showing calcium atoms (green spheres) and the phosphorylcholine molecule (sticks). **E**: Predicted site geometry of the U-CRP complex upon uranyl cation and water molecule binding. Once bound, the uranyl ion prevents the phosphorylcholine molecule from docking with CRP. [Color figure can be viewed in the online issue, which is available at wileyonlinelibrary.com.]

level was 65 RU in the association stage, corresponding to 13% of CRP pentamer.

At a stoichiometry of 2 to 4 uranyl ions per pCRP an inhibition of PC-BSA binding between 60% and 80% at 2 μM UO_2^{2+} was observed [Fig. 4(B)]. The PC-BSA binding level was in any case fully restored in the cycle without UO_2^{2+} immediately following the 2 μM UO_2^{2+} cycle.

This showed that immobilized pCRP did not monomerize into mCRP upon UO_2^{2+} binding, since this conformational change is irreversible and mCRP is known not to bind PC. Additionally, absolute variation of baseline on the pCRP surface was within 3 RU indicating stability of the immobilized material. Since PC-BSA was never in direct contact with UO_2^{2+} in Figure 4(B) experiment, it can be concluded that this inhibition was due solely to the uranyl ion interfering at the CRP calcium binding site rather than any interaction with the phosphate group of PC.

Direct UO_2^{2+} binding to CRP

The availability of high sensitivity SPR instrument, such as Biacore T100 has opened the way to the direct measurement of small ligand interaction. The direct binding of UO_2^{2+} to CRP could be directly assessed on immobilized CRP.

A strong nonspecific interaction for CM-dextran was observed on all sensorchips. As shown in Figure 5, the signal for a pCRP-grafted surface (3190RU of immobilized pCRP) was comparable to that of a nonfunctionalized CM-dextran surface. Nonspecific signal thus originated largely from the interaction of the uranyl ion with negatively charged side-chains or nonfunctionalized dextran carboxylate groups. Nonspecific binding was best fit using a

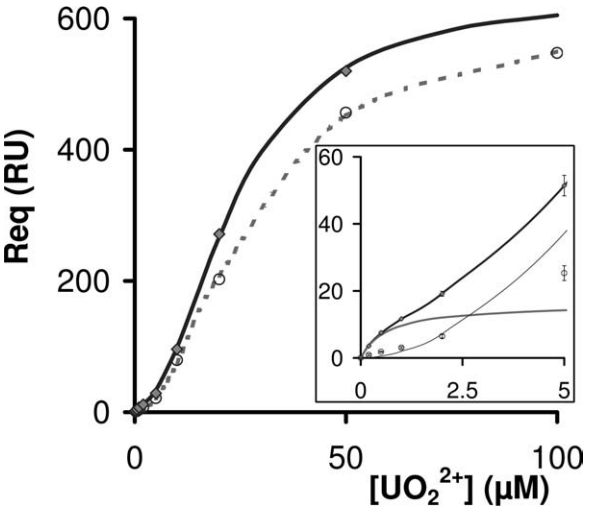

Figure 5. UO_2^{2+} binding SPR signal. SPR signal for UO_2^{2+} binding on a pCRP surface (grey diamonds) compared to the nonspecific signal (NS) measured on a non-functionalized CM-dextran surface (open circles). Both signals are blank subtracted. The best fit of NS was obtained with a four-parameter logistic function (dashed grey line). An additional one-site binding function was necessary [Eq. (2)] for nonlinear fitting of the UO_2^{2+} binding signal on pCRP (black line). **Inset**: Focus on the fitted UO_2^{2+} binding signal on pCRP. The nonspecific contribution modeled with a four-parameter logistic curve (thin black line), the specific binding signal (dark grey line) and the fitted sum (black line) are shown.

four-parameter logistic curve, with an EC50 of 20 μM and a HillSlope of 1.9, indicating positive binding cooperativity.

The overall signal was modeled as the sum of both a standard one-site binding curve and a nonspecific logistic curve as in Eq. (2).

$$Y = Y_{\text{Specific}} + Y_{NS} = \frac{R_{\max} \times X}{K_D + X} + \left(Bottom + \frac{Top - Bottom}{1 + \left(\frac{10^{\text{LogEC}_{50}}}{10^X} \right)^{\text{HillStope}}} \right) \quad (2)$$

By subtracting the nonspecific component from the overall signal, we could access to the specific feature of UO_2^{2+}-pCRP binding. The resulting fit is shown in Figure 5 inset, with a very good absolute sum of squares at 0.08. The corresponding K_D value for the one site binding model was $(6.8 \pm 0.9) \times 10^{-7}$ M. The fitted $R_{\max}$ value at 16.2 RU was in agreement with the expected $R_{\max}$ [$(\text{RUpred})_{\max}$], given the quantity of CRP immobilized on the sensor chip, at 25 RU (CRP subunits, RII corrected), indicating that UO_2^{2+} binds about 65% of CRP calcium sites with high affinity in buffer containing 50 μM $CaCl_2$.

Discussion

Experimental validation of computational prediction is unfortunately seldom achieved for a number of reasons including the difficulty in accessing biological materials. We had this requirement in mind in the design of this study. Our docking tool for UO_2^{2+} proposed several targets, and multiple binding sites in proteins. The performance of the method had to be confirmed and we selected a demonstrative example. The fact that UO_2^{2+} could interfere with the Ca^{2+} binding pocket of CRP, and consequently inhibit PC binding to CRP is original and pertinent from a toxicological point of view. Experimental results supported the predicted binding of UO_2^{2+} at the specific binding site for calcium, with an unexpectedly high affinity, about 100-fold higher than that of calcium.

The colocalization of calcium and uranyl cations was confirmed by examining the selective inhibition of the pronase-sensitive calcium binding loop of CRP. Electrophoresis experiments showed that UO_2^{2+} was at least 10-fold more efficient than calcium in protecting CRP from digestion. Maldi-TOF results were also in agreement with this finding. Magnesium did not inhibit proteolysis, which rules out a nonspecific electrostatic mechanism. As seen in Figure 3(C), CRP showed slightly delayed band migration, but only at higher uranyl ion concentrations. This was considered an artifact due to silver staining since it was not observed on coomassie blue staining gels performed in parallel (Invitrogen NuPAGE Novex 10% Bis-Tris Mini gels, Supporting Information, Fig. S3). The stoichiometry of 0.9 UO_2^{2+} per CRP subunit observed in ICP-MS experiments further indicated that the uranyl ion binds in the calcium binding site, one uranyl cation replacing both calcium cations.

We measured a dissociation parameter (K_D) of 0.68 μM for the interaction between CRP and UO_2^{2+} in the presence of 50 μM Ca^{2+}. Thus, UO_2^{2+} binds to native pCRP with an affinity one-hundred fold higher than calcium, since the K_D for calcium was reported to be in the range of 50–78.1 μM. Ionized calcium concentration in interstitial fluid or plasma is about 1.2 mM,[45] so a competition with the uranyl ion could be expected as soon as its local concentration exceeds 10 μM. Moderate UO_2^{2+} intoxication might be sufficient to hinder CRP adhesion to apoptotic or pathogen cells. Internal contamination with uranium is often associated with inflammation[47,48] and CRP levels might thus increase up to 1000 fold. CRP could then constitute a biochemical cargo for uranium in the serum. However, UO_2^{2+} concentrations in interstitial fluids are probably as transient as blood concentrations, so biological relevance of these dynamic processes is difficult to estimate without *in vivo* experiments.

In addition to these biochemical investigations, we examined atoms appearing in the first coordination shell of uranium. Existing data are extracted from resolved protein structures where the uranyl cation was used for phase resolution in multiple isomorphous replacement,[19,49] and have also been documented for transferrin.[6] We propose here the direct binding of a uranyl cation with protein side-chain atoms only as first shell ligands, apart from one water molecule, as observed in almost all UO_2^{2+} sites found in the Protein DataBank. Interestingly, Gln150 is reported here among coordinating groups in UO_2^{2+} first-sphere. The glutamine amide oxygen atom had not been reported before as a direct uranyl ion ligand, although amide oxygen atoms are likely UO_2^{2+} chelators since they are reported as hard Lewis bases according to the hard/soft acid/base theory (HSAB).

Our detection methodology was used with a particular focus on molecular interactions. Strikingly, the first selected and tested target has a calcium site prone to UO_2^{2+} competition. Such calcium binding sites favoring pentagonal or hexagonal planar chelation geometry, as needed for the uranyl ion complexation, may account for the chemical toxicity of UO_2^{2+} and its distribution in tissues.

Material and Methods

The screening methodology was detailed previously.[19] Briefly, a first shell environment of the uranyl cation is drawn from the statistical analysis of structures of complexes from the Cambridge

Structural Databank (CSD) and the PDB. UO_2^{2+} is placed at each node of a grid laid over the PDB structure in a first geometrical screening stage, and all possible binding oxygen atoms from the protein are tentatively moved towards the expected UO_2^{2+} first shell positions, using side-chain rotamers for maximum flexibility. When this stage is favorable, a second stage involving energy minimization in the Amber force-field is applied, allowing the calculation of a score estimating the total energy of the protein-metal complex [Fig. 1 Top right].

This method was applied to a nonredundant subset of the PDB, prepared to focus on the most biologically pertinent protein structures and reduce computer screening time. PDB sequences aligning with the same areas of native Swiss-Prot sequences were gathered by performing a hierarchical clustering of PDB chains based on a UniProtKB-Swiss-Prot versus PDB blast. A C-alpha RMSD was then calculated in each cluster, relative to the least mutated PDB chain compared with the accession number (AC), to retain as many alternative conformation structures as needed. The least mutated PDB entry, compared with the native sequence, was then kept in each subcluster. 12837 PDB unique IDs were selected as the database subset [Fig. 1 Top].

An automated version of our INTERALIGN program[50] was used for sequence manipulations and C-alpha RMSD calculations for sequence alignments originating in the Basic Local Alignment Search Tool (BLAST). The computing time to process the PDB subset files was equivalent to 625 days on a single 3.2 GHz Pentium IV with 1024M RAM running with Linux. Database collection and processing was performed early in this work, using December 2005 version for the PDB database and March 2005 version for the SMID database (Biomolecular Object Network Databank,[51]).

Choice of C-reactive protein

The selection of proteins of interest [Table I] was based solely on scores and redundancy. Proteins with at least one predicted UO_2^{2+} site with a score below −500 were selected. This threshold corresponds to the mean +1SD value of the specific population distribution (84% of specific scores). Score spreading of sites per PDB entry was followed to control the number of nonspecific hits, since detected chelation areas involving common residues predominantly yield similar score levels. Proteins selected in Table I counted at least two associated structures, showed a mean value of scores below −600, a standard deviation (SD) below 100, less than 31.6% of scores higher than mean + 1SD (the expected percentage for a normal score distribution is 15.8%, 2 times as a safety coefficient), and at least one SMID ligand less than 3 Å form the uranyl ion site. We then focused on proteins interacting with molecules in a metal-dependent fashion, with an apo-form of the protein structure available to check on conformational stability compared to the metal loaded structure. This led to the selection of the calcium mediated CRP/phosphorylcholine interaction.

Reagents

UO_2^{2+} speciation and solubility were carefully monitored for the experimental setup since neutral pH tends to form precipitates of UO_2^{2+}-hydroxyl. In accordance with Jang *et al.* who studied schoepite [$UO_2(OH)_2.H_2O(c)$] formation at pH 7,[52] we kept UO_2^{2+} concentration below 1 and 0.1 mM for electrophoresis and SPR experiments, respectively. All the experiments were performed within 1 day, from extemporaneous dilutions of the stock solution. The UO_2^{2+} stock solution was 100 mM UO_2^{2+} diacetate, pH = 4.

Pronase from *Streptomyces griseus* (Calbiochem, La Jolla #537088) was freeze-dried, and CRP (Biospacific, Emeryville, #J81600135) was solubilized in 20 mM Tris-HCl (pH = 7.5), 2 mM $CaCl_2$, 140 mM NaCl, and 0.05% NaN_3. Monomeric CRP (mCRP) was prepared according to the urea method from Potempa *et al.*[34]

Unless otherwise indicated all chemical products were from Sigma-Aldrich (St-Quentin Fallavier, France) and used without further treatment. Pure water was provided by a DirectQ purification system (Millipore, Billerica).

Pronase assay

a. Pronase/CRP ratios: 24 μg of a CRP solution at 1 mg/mL were dialyzed against 10 mM Tris-HCl and 150 mM NaCl, pH 7, using a Micro DispoDialyzer (Harvard Apparatus, Holliston). Four 30 μL CRP samples (200 μg/mL, 10 mM Tris-HCl, 150 mM NaCl, pH 7) were incubated with 1mM $CaCl_2$ (1 h at RT), then digested (2 h at 37°C) with pronase [1 mg/mL in Tris-Buffered Saline (TBS)] at various protease/substrate ratios (1% to 10%, W/W).
b. Calcium protection: 1 mg/mL CRP solution was dialyzed in 25 mM Hepes, 75 mM NaCl, pH 7, then adjusted to 200 μg/mL. The protein solution was distributed (30 μL) and incubated (1 h at RT) with $CaCl_2$ concentrations ranging from 1 to 10 mM. The samples were digested by pronase (5% W/W, 2 h, 37°C).
c. UO_2^{2+} protection: the preparation was identical to the previous calcium experiments, with UO_2^{2+} concentrations ranging from 0.1 to 1 mM to prevent UO_2^{2+} hydrolysis and precipitation in pH 7 buffer.

Pronase reactions were stopped by cooling in ice and the digests were immediately analysed by SDS-

PAGE, using a PhastSystem (GE Healthcare, Buc, France) with precast gradient gels PhastGel™ 8-25 and SDS buffer strips, according to the manufacturer's instructions. SeeBlue® Plus2 prestained standards were from Invitrogen (Cergy Pontoise, France).

SDS-PAGE analyses were carried out on duplicates from the different digests, and the gels were silver stained. SDS was added to each sample before heating (90°C, 10 min), but no DTT since it induces a smear on gels in the presence of UO_2^{2+}.

MALDI-TOF-MS assays

MALDI-TOF-MS spectra were recorded on a MALDI-TOF Biflex IV mass spectrometer (Bruker Daltonics) in positive ionization mode. Sinapinic acid prepared as saturated solution in 30% acetonitrile, 70% milli-Q water, and 0.1% trifluoroacetic acid was used as matrix for desalted unproteolyzed proteins. A CRP solution at 1 mg/mL was extensively dialyzed against 10 mM Tris-HCl and 150 mM NaCl, pH 7.4, using a Micro DispoDialyzer. Protein samples (500 μg/mL) were distributed in three glass vials (27 μL), with an added volume of 3 μL of water, $CaCl_2$ (1 mM final concentration) or UO_2^{2+} (100 μM final concentration) before incubation (1 h, RT). Digestion (2 h at 37°C) with pronase (1 mg/mL solution in TBS) was at a protease/substrate ratio of 5% W/W. Finally, 30 μL of ethanol were added in each sample followed by sonication. Samples of 0.5 μL were spotted onto a Scout MALDI 384 target (Bruker Daltonics) using dried droplet method, with the addition of 0.5 μL of sinapinic acid. Spectra were acquired in linear mode (150–250 laser shots) in the m/z range from 5000 to 30,000. Higher masses were also scrutinized to check for the absence of multimeric CRP. Calibration was achieved using standard I from Bruker (insulin, ubiquitin, cytochrom C, myoglobin peaks), and the expected average mass of CRP (23047.32 Da).

ICP-MS assay

To load CRP with UO_2^{2+}, a 1 mg/mL CRP sample was first dialyzed against 200 mL 150 mM NaCl, 10 mM acetate buffer using a Micro DispoDialyzer (Harvard Apparatus, Holliston). Then the sample was diluted in the same buffer with added UO_2^{2+} diacetate to reach a final concentration before dialysis (10000 daltons cutoff) of 10 μM protein and 100 μM UO_2^{2+}. A sample with 100 μM UO_2^{2+} without protein was also dialyzed in the same buffer as a reference. The buffer pH was adjusted to five to insure UO_2^{2+} solubility at a concentration up to 100 μM for an overnight run (see Supporting Information Figure S4 and Table SIII). Two 100 μL samples were then dialyzed (10000 daltons cutoff) overnight with 200 mL buffer without UO_2^{2+}. The CRP concentration was readjusted using a CRP extinction coefficient (mg/mL) of 1.818 using a Carry 300 spectrophotometer (Varian) for 280 nm absorbance measurements. Two hundred microliters of UO_2^{2+} loaded samples were diluted in 5% HNO3 before ICP-MS analysis (PQ Excell Option S, Thermoptek)

SPR assays

Experiments were performed on a Biacore T100 instrument (GE Healthcare). UO_2^{2+} mass is above the reported sensitivity of this instrument, making UO_2^{2+} binding measurements possible. However, nonspecific binding and refractive index increment need to be taken into account for accurate measurements as detailed in this work.

Free phosphorylcholine was from Sigma-Aldrich and phosphorylcholine conjugated to BSA (10 PC per BSA, functionalized on Tyr residues) was from Biosearch Technologies (Novato). PC-BSA, pCRP, and mCRP were immobilized on CM5 sensor chips using standard amine-coupling EDC/NHS chemistry followed by ethanolamine deactivation of activated CM-dextran groups. A blank flow cell was used as a reference on all chips.

The running buffer was a 10 mM Tris, 150 mM NaCl, and 50 μM $CaCl_2$ solution without EDTA. No surfactant, such as Tween 20, was used in the running buffer since binding levels of CRP to PC-BSA in the presence of calcium were 10 times higher in the absence of detergent, with no measurable adverse effect on nonspecific binding. Calcium concentration was adjusted to 50 μM to maintain a CRP/calcium ratio slightly higher than that of the CRP long storage manufacturer solution (1 mg/mL CRP with 2 mM calcium) at CRP concentrations up to 1000 nM.

The regeneration buffer was 10 mM NaOH, 0.05% SDS, 0.5% Tween20 and 2mM EDTA, ensuring stable baseline, reproducible binding levels and minimal nonspecific binding, under all conditions.

The full SPR cycle of the uranyl ion capture experiments is given in Figure 4(B,C) and Supporting Information Figure S2. The stages were: UO_2^{2+} diacetate capture (120 sec, 10 μL/min.), dissociation/wash in running buffer (115 sec, 30 μL/min), then injection of 100 nM PC-BSA diluted in the running buffer with or without UO_2^{2+}, dissociation and regeneration.

All SPR data were analyzed using Biacore T100 evaluation software version 1.1 (GE Healthcare). Fits were performed using an MW of 115 kDa for pCRP, 70 kDa for PC-BSA, and 23 kDa for mCRP.

The predicted maximum instrument responses for binding of a single ligand $(RUpred)_{max}$ were estimated using the standard formula $(RUpred)_{max} = RU_M \times (MW_L/MW_M)$ where RU_M is the signal corresponding to the immobilized molecule, MW_L is the molecular weight of the ligand or analyte (i.e., the circulating molecule) and MW_M is the molecular weight of the immobilized molecule. Davis and

Wilson[46] report that correction of this formula to account for RII differences between immobilized molecule and ligand might be needed for avoid errors reaching a factor of 2 on stoichiometry predictions. We used a bare gold surface to estimate UO_2^{2+} RII value using SPR.[53]

Equation 2 was entered in Graphpad Prism version 4.00 (GraphPad Software, San Diego California, www.graphpad.com), which was used for nonlinear fitting of data.

Structures were drawn with DS Visualizer 2.0 (Accelrys Software) and rendered with POV-Ray 3.6 under Linux (Persistence of Vision Pty. 2004).

Acknowledgments

This work was partly supported by the programme Toxicologie Nucléaire Environnementale of CEA.

References

1. Yamashita MM, Wesson L, Eisenman G, Eisenberg D (1990) Where metal ions bind in proteins. Proc Natl Acad Sci USA 87:5648–5652.
2. Nayal M, Di Cera E (1994) Predicting Ca(2+)-binding sites in proteins. Proc Natl Acad Sci USA 91:817–821.
3. Dudev T, Lim C (2003) Principles governing Mg, Ca, and Zn binding and selectivity in proteins. Chem Rev 103:773–787.
4. Harding MM (2004) The architecture of metal coordination groups in proteins. Acta Crystallogr D 60: 849–859.
5. Hartsock WJ, Cohen JD, Segal DJ (2007) Uranyl acetate as a direct inhibitor of DNA-binding proteins. Chem Res Toxicol 20:784–789.
6. Vidaud C, Gourion-Arsiquaud S, Rollin-Genetet F, Torne-Celer C, Plantevin S, Pible O, Berthomieu C, Quemeneur E (2007) Structural consequences of binding of UO_2^{2+} to apotransferrin: can this protein account for entry of uranium into human cells? Biochemistry 46:2215–2226.
7. Teulon JM, Parot P, Odorico M, Pellequer JL (2008) Deciphering the energy landscape of the interaction uranyl-DCP with antibodies using dynamic force spectroscopy. Biophys J 95:L63–L65.
8. Wegner SV, Boyaci H, Chen H, Jensen MP, He C (2009) Engineering a uranyl-specific binding protein from NikR. Angew Chem Int Ed 48:2339–2341.
9. Vidaud C, Dedieu A, Basset C, Plantevin S, Dany I, Pible O, Quemeneur E (2005) Screening of human serum proteins for uranium binding. Chem Res Toxicol 18:946–953.
10. Basset C, Dedieu A, Guerin P, Quemeneur E, Meyer D, Vidaud C (2008) Specific capture of uranyl protein targets by metal affinity chromatography. J Chromatogr A 1185:233–240.
11. Dedieu A, Berenguer F, Basset C, Prat O, Quemeneur E, Pible O, Vidaud C (2009) Identification of uranyl binding proteins from human kidney-2 cell extracts by immobilized uranyl affinity chromatography and mass spectrometry. J Chromatogr A 1216:5365–5376.
12. Prat O, Berenguer F, Steinmetz G, Ruat S, Sage N, Quemeneur E (2010) Alterations in gene expression in cultured human cells after acute exposure to uranium salt: involvement of a mineralization regulator. Toxicol in Vitro 24:160–168.
13. Leggett RW (1994) Basis for the ICRP's age-specific biokinetic model for uranium. Health Phys 67:589–610.
14. Le Clainche L, Vita C (2006) Selective binding of uranyl cation by a novel calmodulin peptide. Environ Chem Lett 4:45–49.
15. Schymkowitz JW, Rousseau F, Martins IC, Ferkinghoff-Borg J, Stricher F, Serrano L (2005) Prediction of water and metal binding sites and their affinities by using the Fold-X force field. Proc Natl Acad Sci USA 102: 10147–10152.
16. Deng H, Chen GT, Yang W, Yang JJ (2006) Predicting calcium-binding sites in proteins—A graph theory and geometry approach. Proteins-Struct Funct Bioinformatics 64:34–42.
17. Wang X, Kirberger M, Qiu FS, Chen GT, Yang JJ (2009) Towards predicting Ca2+-binding sites with different coordination numbers in proteins with atomic resolution. Proteins-Struct Funct Bioinformatics 75: 787–798.
18. Wang C, Vernon R, Lange O, Tyka M, Baker D (2010) Prediction of structures of zinc-binding proteins through explicit modeling of metal coordination geometry. Protein Sci 19:494–506.
19. Pible O, Guilbaud P, Pellequer JL, Vidaud C, Quemeneur E (2006) Structural insights into protein-uranyl interaction: towards an in silico detection method. Biochimie 88:1631–1638.
20. Barondeau DP, Getzoff ED (2004) Structural insights into protein-metal ion partnerships. Curr Opin Struc Biol 14:765–774.
21. Babor M, Greenblatt HM, Edelman M, Sobolev V (2005) Flexibility of metal binding sites in proteins on a database scale. Proteins 59:221–230.
22. Berman HM, Westbrook J, Feng Z, Gilliland G, Bhat TN, Weissig H, Shindyalov IN, Bourne PE (2000) The Protein Data Bank. Nucleic Acids Res 28:235–242.
23. Snyder KA, Feldman HJ, Dumontier M, Salama JJ, Hogue CW (2006) Domain-based small molecule binding site annotation. BMC Bioinformatics 7:152.
24. Bairoch A, Bougueleret L, Altairac S, Amendolia V, Auchincloss A, Puy GA, Axelsen K, Baratin D, Blatter MC, Boeckmann B, Bollondi L, Boutet E, Quintaje SB, Breuza L, Bridge A, Saux VBL, deCastro E, Ciampina L, Coral D, Coudert E, Cusin I, David F, Delbard G, Dornevil D, Duek-Roggli P, Duvaud S, Estreicher A, Famiglietti L, Farriol-Mathis N, Ferro S, Feuermann M, Gasteiger E, Gateau A, Gehant S, Gerritsen V, Gos A, Gruaz-Gumowski N, Hinz U, Hulo C, Hulo N, Innocenti A, James J, Jain E, Jimenez S, Jungo F, Junker V, Keller G, Lachaize C, Lane-Guermonprez L, Langendijk-Genevaux P, Lara V, Le Mercier P, Lieberherr D, Lima TD, Mangold V, Martin X, Michoud K, Moinat M, Morgat A, Nicolas M, Paesano S, Pedruzzi I, Perret D, Phan I, Pilbout S, Pillet V, Poux S, Pozzato M, Redaschi N, Reynaud S, Rivoire C, Roechert B, Sapsezian C, Schneider M, Sigrist C, Sonesson K, Staehli S, Stutz A, Sundaram S, Tognolli M, Verbregue L, Veuthey AL, Vitorello C, Yip L, Zuletta LF, Apweiler R, Alam-Faruque Y, Barrell D, Bower L, Browne P, Chan WM, Daugherty L, Donate ES, Eberhardt R, Fedotov A, Foulger R, Frigerio G, Garavelli J, Golin R, Horne A, Jacobsen J, Kleen M, Kersey P, Laiho K, Legge D, Magrane M, Martin MJ, Monteiro P, O'Donovan C, Orchard S, O'Rourke J, Patient S, Pruess M, Sitnov A, Whitefield E, Wieser D, Lin Q, Rynbeek M, di Martino G, Donnelly M, van Rensburg P, Wu C, Arighi C, Arminski L, Barker W, Chen YX, Crooks D, Hu ZZ, Hua HK, Huang HZ, Kahsay R, Mazumder R, McGarvey P, Natale D, Nikolskaya AN, Petrova N, Suzek B,

Vasudevan S, Vinayaka CR, Yeh LS, Zhang J (2008) The Universal Protein Resource (UniProt). Nucleic Acids Res 36:D190–D195.
25. Martin ACR (2005) Mapping PDB chains to UniProtKB entries. Bioinformatics 21:4297–4301.
26. Domingues FS, Rahnenfuhrer J, Lengauer T (2007) Conformational analysis of alternative protein structures. Bioinformatics 23:3131–3138.
27. Lesk AM, Chothia C (1980) How different amino-acid-sequences determine similar protein structures—Structure and evolutionary dynamics of the globins. J Mol Biol 136:225–270.
28. Gewurz H, Zhang XH, Lint TF (1995) Structure and function of the pentraxins. Curr Opin Immunol 7: 54–64.
29. Volanakis JE (2001) Human C-reactive protein: expression, structure, and function. Mol Immunol 38: 189–197.
30. Black S, Kushner I, Samols D (2004) C-reactive protein. J Biol Chem 279:48487–48490.
31. Ramadan MA, Shrive AK, Holden D, Myles DA, Volanakis JE, DeLucas LJ, Greenhough TJ (2002) The three-dimensional structure of calcium-depleted human C-reactive protein from perfectly twinned crystals. Acta Crystallogr D Biol Crystallogr 58:992–1001.
32. Shrive AK, Cheetham GM, Holden D, Myles DA, Turnell WG, Volanakis JE, Pepys MB, Bloomer AC, Greenhough TJ (1996) Three dimensional structure of human C-reactive protein. Nat Struct Biol 3:346–354.
33. Thompson D, Pepys MB, Wood SP (1999) The physiological structure of human C-reactive protein and its complex with phosphocholine. Structure 7:169–177.
34. Potempa LA, Siegel JN, Fiedel BA, Potempa RT, Gewurz H (1987) Expression, detection and assay of a neoantigen (Neo-Crp) associated with a free, human C-Reactive protein subunit. Mol Immunol 24: 531–541.
35. Dong AC, Caughey WS, Duclos TW (1994) Effects of calcium, magnesium, and phosphorylcholine on secondary structures of human C-reactive protein and serum amyloid-P component observed by infrared-spectroscopy. J Biol Chem 269:6424–6430.
36. Wu Y, Ji SR, Wang HW, Sui SF (2002) Study of the spontaneous dissociation of rabbit C-reactive protein. Biochemistry-Moscow 67:1377–1382.
37. Tanaka T, Robey FA (1983) A new sensitive assay for the calcium-dependent binding of C-Reactive protein to phosphorylcholine. J Immunol Methods 65:333–341.
38. Lee RT, Takagahara I, Lee YC (2002) Mapping the binding areas of human C-reactive protein for phosphorylcholine and polycationic compounds—relationship between the two types of binding sites. J Biol Chem 277:225–232.
39. Heegaard NHH, Robey FA (1993) A capillary electrophoresis-based assay for the binding of Ca^{2+} and phosphorylcholine to human C-Reactive protein. J Immunol Methods 166:103–110.
40. Christopeit T, Gossas T, Danielson UH (2009) Characterization of Ca2+ and phosphocholine interactions with C-reactive protein using a surface plasmon resonance biosensor. Anal Biochem 391:39–44.
41. Kinoshita CM, Ying SC, Hugli TE, Siegel JN, Potempa LA, Jiang H, Houghten RA, Gewurz H (1989) Elucidation of a protease-sensitive site involved in the binding of calcium to C-Reactive protein. Biochemistry 28: 9840–9848.
42. Gotschli.Ec, Edelman GM (1967) Binding properties and specificity of C-reactive protein. Proc Natl Acad Sci USA 57:706–712.
43. Anderson JK, Stroud RM, Volanakis JE (1978) Studies on binding specificity of human C-reactive protein for phosphorylcholine. Fed Proc 37:1495.
44. Agrawal A, Xu YY, Ansardi D, Macon KJ, Volanakis JE (1992) Probing the phosphocholine-binding site of human C-Reactive protein by site-directed mutagenesis. J Biol Chem 267:25352–25358.
45. Foghandersen N, Altura BM, Altura BT, Siggaardandersen O (1995) Composition of Interstitial Fluid. Clin Chem 41:1522–1525.
46. Davis TM, Wilson WD (2000) Determination of the refractive index increments of small molecules for correction of surface plasmon resonance data. Anal Biochem 284:348–353.
47. Gazin V, Kerdine S, Grillon G, Pallardy M, Raoul H (2004) Uranium induces TNF alpha secretion and MAPK activation in a rat alveolar macrophage cell line. Toxicol Appl Pharm 194:49–59.
48. Monleau M, De Meo M, Paquet F, Chazel V, Dumenil G, Donnadieu-Claraz M (2006) Genotoxic and inflammatory effects of depleted uranium particles inhaled by rats. Toxicol Sci 89:287–295.
49. Van Horn JD, Huang H (2006) Uranium(VI) bio-coordination chemistry from biochemical, solution and protein structural data. Coord Chem Rev 250:765–775.
50. Pible O, Imbert G, Pellequer JL (2005) INTERALIGN: interactive alignment editor for distantly related protein sequences. Bioinformatics 21:3166–3167.
51. Alfarano C, Andrade CE, Anthony K, Bahroos N, Bajec M, Bantoft K, Betel D, Bobechko B, Boutilier K, Burgess E, Buzadzija K, Cavero R, D'Abreo C, Donaldson I, Dorairajoo D, Dumontier MJ, Dumontier MR, Earles V, Farrall R, Feldman H, Garderman E, Gong Y, Gonzaga R, Grytsan V, Gryz E, Gu V, Haldorsen E, Halupa A, Haw R, Hrvojic A, Hurrell L, Isserlin R, Jack F, Juma F, Khan A, Kon T, Konopinsky S, Le V, Lee E, Ling S, Magidin M, Moniakis J, Montojo J, Moore S, Muskat B, Ng I, Paraiso JP, Parker B, Pintilie G, Pirone R, Salama JJ, Sgro S, Shan T, Shu Y, Siew J, Skinner D, Snyder K, Stasiuk R, Strumpf D, Tuekam B, Tao S, Wang Z, White M, Willis R, Wolting C, Wong S, Wrong A, Xin C, Yao R, Yates B, Zhang S, Zheng K, Pawson T, Ouellette BFF, Hogue CWV (2005) The biomolecular interaction network database and related tools 2005 update. Nucleic Acids Res 33:D418–D424.
52. Jang JH, Dempsey BA, Burgos WD (2006) Solubility of schoepite: comparison and selection of complexation constants for U(VI). Water Res 40:2738–2746.
53. Tumolo T, Angnes L, Baptista MS (2004) Determination of the refractive index increment (dn/dc) of molecule and macromolecule solutions by surface plasmon resonance. Anal Biochem 333:273–279.